

Detection of UHE gamma rays from the Crab Nebula: Physical Implications

Dmitry Khangulyan,^{1*} Masanori Arakawa,^{1,2} Felix Aharonian^{3,4,5}

¹*Department of Physics, Rikkyo University, Nishi-Ikebukuro 3-34-1, Toshima-ku, Tokyo 171-8501, Japan*

²*Astrophysical Big Bang Laboratory, RIKEN, Saitama 351-0198, Japan*

³*Dublin Institute for Advanced Studies, School of Cosmic Physics, 31 Fitzwilliam Place, Dublin 2, Ireland*

⁴*Max-Planck-Institut für Kernphysik, Saupfercheckweg 1, 69117 Heidelberg, Germany*

⁵*National Research Nuclear University (MEPHI), Kashirskoje shosse, 31, Moscow 115409, Russia*

Accepted XXX. Received YYY; in original form ZZZ

ABSTRACT

The Crab Nebula is an extreme particle accelerator boosting the energy of electrons up to a few PeV (10^{15} eV), close to the maximum energy allowed by theory. The physical conditions in the acceleration site and the nature of the acceleration process itself remain highly uncertain. The key information about the highest energy accelerated particles is contained in the synchrotron and inverse Compton (IC) channels of radiation at energies above 1 MeV and 100 TeV, respectively. The recent report of detection of ultra-high energy gamma-ray signal from the Crab Nebula up to 300 TeV allows one to determine the energy distribution of the highest energy electrons and to derive the magnetic field strength in the acceleration region, $B \leq 120 \mu\text{G}$, in a parameter-free way. This estimate brings new constraints on the properties of non-thermal particle distributions and puts important constraints on the MHD models for the Crab Nebula, in particular on the feasible magnetization and anisotropy of the pulsar wind. The calculations of synchrotron and IC emission show that future observations with instruments allowing detection of the Crab Nebula above 300 TeV and above 1 MeV will clarify the conditions allowing acceleration of electrons beyond PeV energies in the Crab Nebula. In particular, one will (1) verify the hypothetical multi-component composition of the electron energy distribution, and (2) determine the magnetic field strength in the regions responsible for the acceleration of PeV electrons.

Key words: acceleration of particles – radiation mechanisms: non-thermal – gamma-rays: general – stars: neutron

1 INTRODUCTION

The rotation-powered pulsars initiate high energy gamma-radiation in three physically distinct regions called (i) pulsar magnetosphere, (ii) relativistic electron-positron wind, (iii) pulsar wind nebula (PWN). The cold ultrarelativistic pulsar wind originating from the pulsar magnetosphere and carrying almost the entire rotational energy of the pulsar, eventually terminates resulting in the formation of the non-thermal synchrotron and inverse Compton (IC) nebula. The nonthermal emission of PWNe is caused by interactions of relativistic electrons accelerated at the relatively compact regions associated with the termination of the wind. However, because of the diffusive and advective propagation of electrons, the nonthermal radiation typically extends to dis-

tances tens of parsecs. The energy density of the magnetic field in most of PWNe is comparable to the ambient radiation fields. Thus, the energy of relativistic electrons is shared between the synchrotron and IC channels of radiation in fair fractions making PWNe not only effective electron accelerators but also very effective gamma-ray emitters (Aharonian 1995; Aharonian et al. 1997).

The Crab Nebula is unique, but not an archetypical (as often claimed in the literature) representative of PWNe. Its pulsar is much more powerful than the pulsars of most of other PWNe and, surprisingly, the Crab Nebula is unusually compact. The magnetic field in the Crab Nebula exceeds, by an order of magnitude or more, the typical ($\sim 10 \mu\text{G}$) strength of the magnetic field in other PWNe. Correspondingly the energy density of the magnetic field exceeds by two or three orders of magnitude the radiation fields, thus violating the balance between the synchrotron and IC radiation

* E-mail: d.khangulyan@rikkyo.ac.jp

channels. This makes the Crab Nebula a rather inefficient gamma-ray emitter. The low IC radiation efficiency is compensated by the vast rotational power of the Crab pulsar. Therefore, despite the low efficiency, the Crab Nebula remains a very strong gamma-ray source.

The Crab Nebula is characterized by a very broad Spectral Energy Distribution (SED) that spans over 20 decades, from MHz radio wavelengths to ultra high-energy (UHE) gamma-rays. Another unique feature of the Crab Nebula is the extension of its synchrotron radiation to MeV, and, during the flares, to GeV energies (see [Bühler & Blandford 2014](#); [Zanin 2017](#), and references therein), implying that we deal with an extreme accelerator in which the acceleration of electrons proceeds close to the maximum possible rate allowed in ideal magnetohydrodynamic (MHD) configurations ([de Jager et al. 1996](#); [Aharonian et al. 2002](#); [Lyutikov 2010](#)).

Thanks to its proximity, $d \simeq 2$ kpc, and the high spin-down luminosity of the pulsar, $L_{\text{SD}} \simeq 5 \times 10^{38} \text{ erg s}^{-1}$, the Crab Nebula can be studied in great details (see [Hester 2008](#), and references therein). It contains several spectral features and demonstrates complex energy-dependent morphology (see, e.g., [Hester 2008](#); [Weisskopf et al. 2000](#); [Madsen et al. 2015](#); [Yeung & Horns 2019](#); [Abdalla et al. 2019](#)). The size of the Crab Nebula depends on photon energy, which most likely is caused by the energy-dependent cooling times of the parent electrons. This suggests that the particle acceleration occurs in the inner part of the nebula where relativistic pulsar wind terminates. This conclusion contains, however, caveats. Despite intensive theoretical studies and numerical simulations, it is still not clear how the particle acceleration operates at the relativistic shock waves (see [Sironi et al. 2015](#), and references therein). It is not clear which magnetic field strength and its configuration are required for efficient particle acceleration. Non-thermal particles seen in the Crab Nebula may originate from different acceleration sites, not necessary associated with the pulsar wind termination shock (TS). Even if the TS is the major accelerator in the Crab Nebula, the physical conditions should vary considerably depending on the specific region of the pulsar wind TS, as the TS is expected to have a complex non-spherical shape ([Bogovalov & Khangoulyan 2002](#); [Lyubarsky 2002](#)). Thus, it cannot be excluded that several distinct population of particle, which are possibly accelerated by different mechanisms and/or under different condition, coexist in the Crab Nebula ([Aharonian & Atoyan 1998](#); [Lyutikov et al. 2019](#)). Only precise simulations, together with detailed observations, can help to localize the principal regions of particle acceleration ([Olmi et al. 2015](#)).

It has been argued ([Atoyan & Aharonian 1996](#)) that at least two distinct population of electrons should be invoked to explain the broad-band non-thermal emission of the Crab Nebula. The “radio electrons” are responsible for the MHz and GHz synchrotron emission, while the IC up-scattering off soft photons by these electrons results in the gamma-ray component at GeV energies. The modelling of the radio morphology does not constrain the origin of the radio-emitting electrons in the Crab Nebula, and (re)acceleration of these particle in the bulk of the nebula cannot be excluded ([Olmi et al. 2014](#)).

Multi TeV electrons are classified as “wind electrons” ([Atoyan & Aharonian 1996](#)). Assuming that the emitting electrons are injected at the pulsar wind TS and get advected

with the down-stream flow, the extension of the Crab Nebula seen in UV, X-ray, and TeV energy bands ([Madsen et al. 2015](#); [Abdalla et al. 2019](#)) can be adequately reproduced. We may conclude that the TS plays a principal role in the acceleration of multi-TeV electrons and their injection into the nebula.

Formally, a power-law spectrum of “wind electrons” with an exponential cut-off at PeV energies and a hardening (or a break) at sub-TeV energies, together with the additional “radio electrons” can explain the broad-band spectrum of the Crab Nebula over 20 decades. The nonthermal emission of the Crab Nebula has been studied within a simple one-zone approach or using a more appropriate MHD treatment of particle transport in the nebula ([Kennel & Coroniti 1984](#); [de Jager & Harding 1992](#); [Atoyan & Aharonian 1996](#)). As long as it concerns the spectral fits, the conclusions of both approaches are similar (see, e.g., [Meyer et al. 2010](#)). Namely, the cut-off energy in the spectrum of the “wind electrons” is close to one PeV and the spectrum should continue up to $\simeq 5$ PeV, while the average nebular magnetic field is constrained within 100 and 300 μG .

The analysis of the acceleration process responsible for the “wind electrons” poses a few conceptual questions, for example, regarding the maximum attainable electron energy. The magnetic field at the accelerator makes electrons to lose their energy due to synchrotron cooling. If the synchrotron losses dominate as a radiative cooling channel, the product of the maximum attainable energy and the square root of the magnetic field strength, $E_{\text{MAX}} B_{\text{ACC}}^{1/2}$, can be taken as a measure of the accelerator efficiency. The extension of the electron spectrum to PeV energies in the magnetic field exceeding 100 μG , tells us that in the Crab Nebula we deal with an acceleration efficiency approaching to the ideal MHD limit, i.e., the strength of the accelerating electric field gets close to the strength of the magnetic field.

Another important issue of the spectral modelling of the Crab Nebula is related to the so-called Crab flares – intense flashes of synchrotron radiation extending to GeV energies ([Abdo et al. 2011](#); [Tavani et al. 2011](#)). The short variability time scale and the distinct spectral shape of the flaring component require a magnetic field which is significantly larger than the average nebular field, $B \geq 1$ mG, a non-ideal MHD configuration, and/or relativistic motions with large bulk Lorentz factor (see [Bühler & Blandford 2014](#), and references therein). Even under these extreme conditions, the Crab flares require the presence of electrons with energy exceeding a few PeV. The Crab flares are likely to be formed in a region(s) quite different from the site(s) where the steady component of radiation is produced. But in both cases, the acceleration of electrons proceeds with efficiency close or even beyond the ideal MHD limit.

The tough efficiency requirement to the acceleration of the “wind electrons” can be significantly relaxed assuming that another component of electrons is responsible for the multi-MeV gamma-rays. This hypothesis is supported by a non-smooth transition between the INTERNATIONAL GAMMA-RAY ASTROPHYSICS LABORATORY (*INTEGRAL*) and IMAGING COMPTON TELESCOPE (*COMPTEL*) spectra. If this spectral feature is real, then invoking an additional component of electrons with a hard energy distribution one can better reproduce the spectral structure at multi-MeV energies ([Aharonian & Atoyan 1998](#)). The currently available data do not

exclude a significantly stronger magnetic field in the regions where this hypothetical hard distribution is localized (Aharonian & Atoyan 1998). Therefore, the IC emission produced by electrons from the hard component could be suppressed compared to the IC radiation associated with the standard “wind electron” component. The synchrotron radiation alone does not allow one to infer information about the electrons and magnetic fields in this most critical, for highest energy electrons, MeV/GeV energy region. For any reasonable magnetic field, the MeV synchrotron radiation is produced by multi-hundred TeV electrons. Therefore, the UHE gamma-rays produced by the same electrons through the IC scattering contains information which can shed light on both electron energy distribution and magnetic field strength.

In this regard, the recently reported detection of fluxes gamma-rays above 100 TeV (Amenomori et al. 2019; Abeysekara et al. 2019) are of great interest. These measurements significantly extend the spectrum, which previously was measured up to 80 TeV (Aharonian et al. 2004). The emission reported by Tibet Air Show Gamma Experiment (*Tibet ASy*) and High Altitude Water Cherenkov Gamma-Ray Observatory (*HAWC*) collaborations is produced by multi-hundred TeV electrons scattering off the Cosmic Microwave Background Radiation (CMBR) allowing robust constraints on the parent electron spectrum and the magnetic field strength in the region of acceleration. Below we discuss some implications of the new UHE gamma-ray measurements in the context of the highest energy electrons accelerated in the Crab Nebula.

2 UHE PARTICLES IN THE CRAB NEBULA

2.1 Transport

While high-energy particles in PWNe lose their energy due to synchrotron, IC, and adiabatic losses, in the UHE domain synchrotron losses are expected to dominate. The synchrotron cooling time is:

$$t_{\text{SYN}} \approx 4 \times 10^5 E_{\text{PEV}}^{-1} B_{\text{mG}}^{-2} \text{ s}, \quad (1)$$

where E_{PEV} and B_{mG} are the electron energy and magnetic field strength in units of PeV and mG, respectively. The magnetic field in the nebula originates in the pulsar. Its characteristic strength is determined by the distance from the pulsar to the point where the pulsar wind terminates (Rees & Gunn 1974; Kennel & Coroniti 1984). In PWNe, the down-stream magnetic field is changed on scales comparable to the TS radius (see, e.g., Kennel & Coroniti 1984). It is convenient to introduce the so-called dimensionless advection distance:

$$\lambda_{\text{SYN}} = \frac{t_{\text{SYN}} V_{\text{F}}}{R_{\text{TS}}} = \frac{10^{-2}}{B_{\text{mG}}^2 E_{\text{PEV}}} \left(\frac{V_{\text{F}}}{0.3} \right) \left(\frac{R_{\text{TS}}}{0.1 \text{ pc}} \right), \quad (2)$$

where V_{F} is flow velocity in the units of the speed-of-light. The above equation suggests that the emission of UHE > 100 TeV electrons provides good probe for physical conditions in the acceleration region.

2.2 Emission

The synchrotron emission of PeV electrons in a magnetic field of mG scales appears in the gamma-ray energy band:

$$\hbar\omega_{\text{SYN}} \approx 60 E_{\text{PEV}}^2 B_{\text{mG}} \text{ MeV}, \quad (3)$$

The synchrotron radiation alone does not provide independent information about the electrons and the magnetic field. The IC component of radiation of the same electrons allows us to disentangle the strength of the magnetic field and the energy parent electrons.

In the Crab Nebula, several photon fields serve as targets for the IC emission (Atoyan & Aharonian 1996). Three dominant IC components are contributed by the far-infrared (FIR), CMBR, and synchrotron photons. Up-scattering of synchrotron photons through the synchrotron-self-Compton (SSC) channel provides the major contribution at TeV energies. The synchrotron target is however characterized by a relatively high photon energy, therefore in the UHE band the SSC process is significantly suppressed because of the Klein – Nishina (KN) effect. The KN effect becomes substantial when

$$\varepsilon \geq \varepsilon_{\text{KN}} = 3 \times 10^{-4} E_{\text{PEV}}^{-1} \text{ eV}. \quad (4)$$

The flux from the Crab Nebula at these energies is about $10^{-10} \text{ erg s}^{-1} \text{ cm}^{-2}$. For the radius of $R_{\text{N}} \approx 1 \text{ pc}$, the energy density of the synchrotron photons which are up-scattered in the Thomson regime, is $\sim 10^{-2} \text{ eV cm}^{-3}$, significantly below the energy density of the Galactic background photon fields.

If the target is a diluted Plankian radiation, the limit given by Eq. (4) for 100 TeV electrons corresponds to the temperature approximately of 10 K. This implies that all background fields, except the CMBR, are up-scattered deep in the KN regime. Thus, the UHE emission reported by the *Tibet ASy* and *HAWC* collaborations is predominately contributed by the CMBR photons. This conclusion is supported by numerical calculations shown in Fig. 1. The calculations have been performed in framework of one-zone approximation using the package *naima* (Zabalza 2016). The analytic approximation proposed in Aharonian et al. (2010) was used for computing the synchrotron emission. For the SSC component of radiation we used the IC cross-section averaged over the scattering angles (Aharonian & Atoyan 1981), and the IC spectra generated on the Galactic background fields were calculated with an analytic approximation by Khangulyan et al. (2014). The electron distribution was assumed to be a broken power-law with an exponential cutoff:

$$\frac{dN}{dE} = A \exp \left[- \left(\frac{E}{E_{\text{cut}}} \right)^2 \right] \times \begin{cases} \left(\frac{E}{1 \text{ TeV}} \right)^{-\alpha_1} & \text{if } E < E_{\text{br}}, \\ \left(\frac{E_{\text{br}}}{1 \text{ TeV}} \right)^{\alpha_2 - \alpha_1} \left(\frac{E}{1 \text{ TeV}} \right)^{-\alpha_2} & \text{if } E > E_{\text{br}}. \end{cases} \quad (5)$$

Here E is electron energy, A is the normalization constant for the electron spectrum, E_{cut} is the cutoff energy, and E_{br} is power-law break energy. We adopted the following parameters: $E_{\text{cut}} = 1.863 \text{ PeV}$, $E_{\text{br}} = 0.265 \text{ TeV}$, $\alpha_1 = 1.5$, $\alpha_2 = 3.233$ and $B = 125 \mu\text{G}$.

The IC spectra generated by four different photon fields, CMBR, FIR (a graybody distribution with temperature

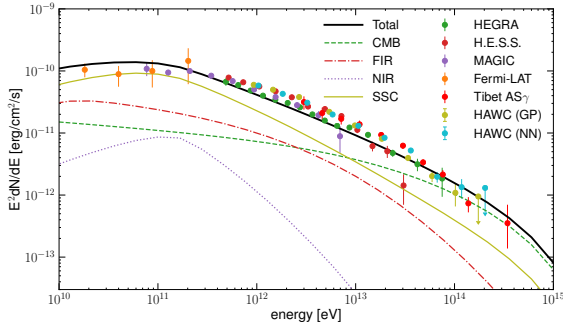


Figure 1. Gamma-ray spectrum of the Crab Nebula. The gamma-ray data are taken from *Fermi*/LAT (Buehler et al. 2012), HEGRA (Aharonian et al. 2004), H.E.S.S. (Aharonian et al. 2006), MAGIC (Albert et al. 2008), *Tibet ASy* (Amenomori et al. 2019), *HAWC* (Abeysekara et al. 2019). IC spectra produced on four different photon fields: SSC (solid line), CMBR (dashed line), FIR (dash-dotted line), and NIR (dotted line) are shown together with their summation (thick solid line).

$T_{\text{FIR}} = 70$ K and energy density $U_{\text{FIR}} = 0.5$ eV cm $^{-3}$, near-infrared (NIR) ($kT_{\text{NIR}} = 5000$ K, $U_{\text{NIR}} = 1$ eV cm $^{-3}$), and synchrotron photons, are shown in Fig. 1. We assumed that the synchrotron target is homogeneously generated in the nebula, and the volume averaged density of the SSC target is enhanced by a factor of 2.24 as compared to the boundary region of the nebula (see Atoyan & Aharonian 1996, for details).

Remarkably, since UHE gamma rays are predominantly produced at scatterings on CMBR photons with precisely known temperature, the spectrum and the total energy of parent electrons can be robustly derived. Using the analytical presentations from Khangulyan et al. (2014), one can conclude the highest energy part of the spectrum reported by *Tibet ASy*, $\hbar\omega \approx 300$ TeV requires electrons of energy up to 0.8 PeV. The corresponding numerical calculations are presented in Fig. 2, where the synchrotron and IC emission by electrons with energy limited to several energy intervals are shown. The overall energy distribution of electrons is assumed to obey Eq. (5).

It is seen that the *Tibet ASy* measurements constrain the electrons in the range 50 – 750 TeV, in a parameter-free way. The calculation of the synchrotron emission from these particles requires additional assumptions on the strength and possible distribution of the magnetic field. In Fig. 3, we show the synchrotron emission from 50 – 750 TeV electrons for three different strengths of the magnetic field as obtained in the framework of a one-zone model (all the remaining model assumptions are the same as in Fig. 2). One can see that the synchrotron emission of ~ 300 TeV electrons (derived model-independently from the *Tibet ASy* measurements), violates the flux level in the MeV band measured with *INTEGRAL* and *COMPTEL*, unless $B \lesssim 125$ μG . To illustrate that these data indeed constraint the strength of the magnetic field with very high accuracy, in Appendix A we present a Markov Chain Monte Carlo (MCMC) simulation of the *INTEGRAL* and gamma-ray (with energy above 10 TeV that include the HEGRA, H.E.S.S. and *Tibet ASy* measurements) spectra with *naima* (Zabalza 2016). Adopt-

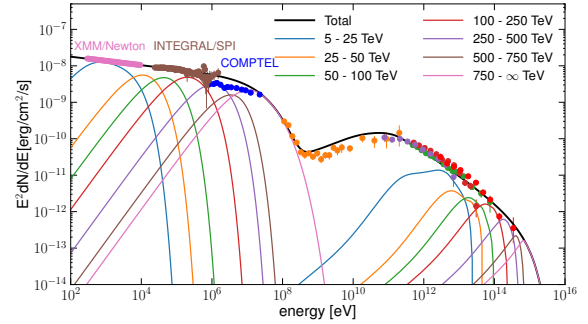


Figure 2. Non-thermal emission computed with a one-zone model (thick solid line). Synchrotron and IC emission by electrons from several energy ranges, 5 – 25 TeV, 25 – 50 TeV, 50 – 100 TeV, 100 – 250 TeV, 250 – 500 TeV, 500 – 750 TeV, ≥ 750 TeV are shown with thin solid lines. The magnetic field was assumed to have a strength of $B = 125$ μG . In addition to the gamma-ray data shown in Fig. 1, the following X-ray and soft gamma-ray measurements are shown *XMM-Newton* (Kirsch et al. 2005), *INTEGRAL/SPI* (Jourdain & Roques 2009), and *COMPTEL* (Kuiper et al. 2001).

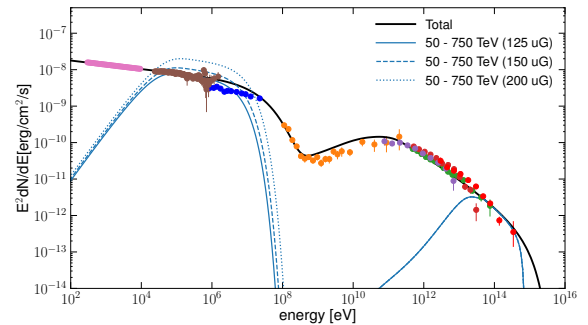


Figure 3. Computed synchrotron emission from electrons with energy in the range from 50 to 750 TeV for three different magnetic field strengths, $B = 125$ (thin solid line), 150 (dashed line), and 200 μG (dotted line). The electron energy distribution was kept unchanged to satisfy the *Tibet ASy* measurements. The synthetic non-thermal spectrum is shown with thick solid line. For the origin of the shown data points see Figs. 1 and 2.

ing a power-law with exponential cutoff energy distribution of the emitting particles (which is a rather good approximation for the relatively narrow relevant energy range), the MCMC simulations require the magnetic field strength to be in the range $B = 118^{+3}_{-2}$ μG , which is consistent with a less sophisticated estimate shown in Fig. 3.

3 DISCUSSION

3.1 Acceleration of UHE electrons

There is an important question related to the radiation models for the Crab Nebula: do these studies allow defining the strength of the magnetic field at the acceleration site? As synchrotron emission components depend on a quantity

$EB^{1/2}$, there is an ambiguity between the particle energy and the magnetic field strength. Thus, the synchrotron spectrum alone does not define the magnetic field strength. Detection of the variability time-scale in the case of the GeV flares allows obtaining a relatively robust estimate for the magnetic field strength. The emission produced by the “wind electrons” is steady, however one can register the IC component emitter by the same particles. It means that that is IC emission that in fact constraints the strength of the magnetic field in the Crab Nebula. Non-thermal particle can escape from the acceleration site and produce their emission in other parts of the source. The physical conditions at the emission site may differ strongly from those of the acceleration site. If for some particle the cooling time is significantly longer than the acceleration time (i.e., the time for which the particle was confined in the accelerator), then its emission allows probing the averaged physical conditions in the source, but not in the accelerator. As high-energy particles are characterized by shorter cooling time, one can constrain the accelerator magnetic field by measuring the synchrotron and IC of the highest energy particles in the source.

As argued above, the study of the synchrotron and IC radiation components associated with UHE electrons provide a powerful tool to constrain the magnetic field at the acceleration site. Indeed, these electrons are expected (i) to lose their energy quickly, thus do not propagate far away from the acceleration site and (ii) interact predominately with CMBR with precisely known distribution and energy density. The recent detection of UHE gamma-rays from the Crab Nebula beyond 100 TeV (Amenomori et al. 2019) resolves the “electron energy – magnetic field strength” ambiguity characterizing the synchrotron channel. This detection allows us to robustly derive the strength of the magnetic field in the region responsible for the acceleration of multi-hundred TeV electrons, $B \leq 120 \mu\text{G}$, in a parameter-free way (see Appendix A).

The obtained limit does not concern the acceleration of PeV electrons. The IC emission of PeV electrons should appear in the spectrum above 400 TeV. Currently, no measurements are available in this energy band. However, it is expected that Large High Altitude Air Shower Observatory (LHAASO), a new powerful cosmic ray facility, will soon probe the gamma-ray spectrum of the Crab Nebula in this energy interval (see He 2019, and references therein). Remarkably, the attenuation of such energetic photons from the Crab due to the interactions with diffuse galactic radiation fields is expected to be not significant (Veretto & Lipari 2016).

The synchrotron spectrum of the Crab Nebula extends to energies beyond 100 MeV and requires electrons with energy up to several PeV. This emission component is conventionally associated with the “wind electrons”, however the gamma-ray spectrum in the 1 to 100 MeV band is not smooth. It shows a structure which can be better reproduced by two different populations of UHE electrons described by power-law distribution with an exponential cut-off ($E_{\text{cut}} = 500 \text{ TeV}$) and by a hard energy distribution peaking at higher energies (Aharonian & Atoyan 1998). The two considered electron populations could be accelerated in different regions through different acceleration processes. The superposition of emission of these two components is demonstrated in Fig. 4. Similarly to Aharonian & Atoyan (1998)

we approximated this additional component with a ultrarelativistic Maxwellian distribution, although we note that this is just a formal approximation, and it does not imply any underlying assumptions regarding the nature of this component (see, however, Atoyan & Nagapetyan 1987). For example, Sironi & Spitkovsky (2014) have shown that a hard distribution of non-thermal particle can be formed by magnetic reconnection in highly magnetized environments. Lyutikov et al. (2019) suggested that an electron component accelerated by magnetic field reconnection operating in the bulk of the nebula (see, e.g., Komissarov 2013) might be responsible for the dominant radio and soft gamma-ray emission detected from the Crab Nebula. Magnetic reconnection is considered as a feasible mechanism to power the Crab flares (Cerutti et al. 2012, 2013; Lyutikov et al. 2018), thus the particles producing the steady MeV and flaring GeV synchrotron emission may have a common origin (see the discussion in Lyutikov et al. 2019). As it is shown below the counterpart IC emission may provide important information to test this possibility.

We show in Fig. 4 synthetic spectra computed for three different strengths of the magnetic field in region where the hard high energy distribution is localized: $B_2 = 125, 500,$ and $1000 \mu\text{G}$. As it can be seen by a suitable choice of the temperature parameter ($E_T = 260, 130,$ and 90 TeV , respectively), one can get identical synchrotron spectra. In contrast, the IC spectra show important differences (see Fig. 4).

First of all, if the MeV spectral feature is real, one should expect a significantly smaller flux at 300 TeV. The expected difference is comparable with the Tibet ASy error, so presently we cannot make any quantitative statement. However, the future measurements LHAASO should allow distinguishing between these two cases (shown with black and gray lines in Fig. 4). To illustrate that, we show in Fig. 4 the LHAASO sensitivity expected for one-year exposure (Bai et al. 2019). We also note that important new information can be obtained, as well, in the MeV energy band, e.g., with Gamma-Ray and AntiMatter Survey (Aramaki et al. 2020) or e-ASTROGAM (de Angelis et al. 2018). If these observations will confirm the two-component composition of the Crab Nebula spectrum, then one can attempt to define the magnetic field strength in the “Maxwellian region”. Although from Fig. 4 it may look as the LHAASO sensitivity is not good enough for such measurements, we remind that the shown sensitivity corresponds to one-year exposure. If the instrument will operate long enough, e.g. ten years, its performance may appear to be sufficient for obtaining a meaningful constraint on the magnetic field strength in this hypothetical “Maxwellian region.”

3.2 On the magnetization of the pulsar wind

Presently, the MHD treatment provides the most fruitful approach for studying the properties of PWNe (Kennel & Coroniti 1984; Bogovalov & Khangouljian 2002; Komissarov & Lyubarsky 2004; Bogovalov et al. 2005; Volpi et al. 2008; Camus et al. 2009; Bucciantini 2014; Porth et al. 2014; Barkov et al. 2019).

The MHD framework provides important insights into non-thermal physical processes in PWNe. In particular, this concerns the dynamics of the magnetic field, particle transport and their radiation. Although the simplest 1D analytic

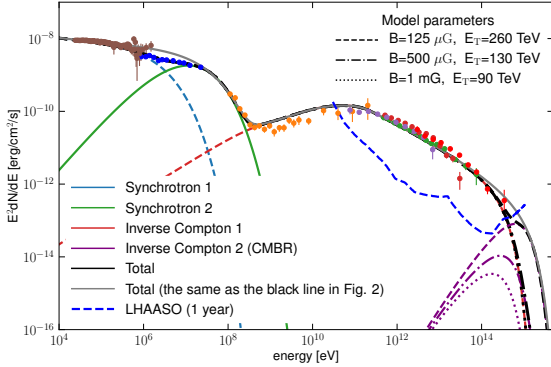


Figure 4. Computed synchrotron and IC emission components produced by two populations of electrons: a power-law with exponential cut-off energy distribution in $B = 125 \mu\text{G}$ magnetic field, and a relativistic Maxwellian in $B = 125, 500,$ and $1000 \mu\text{G}$ fields. For the origin of the shown data points see Figs. 1 and 2.

models helped to advance the studies of PWNe, the most realistic results are achieved with numerical 3D MHD simulations (see, e.g., Porth et al. 2014; Barkov et al. 2019).

The MHD models have limitations among which the phenomenological treatment of particle acceleration is essential. Although it is proved that relativistic outflows on different astrophysical scales are characterized by particle acceleration and radiation, PWNe demonstrate unprecedentedly high efficiency of non-thermal processes. Despite the systematic study of PWNe, it is still not fully understood what makes of PWNe so efficient high-energy sources.

One of the key parameters in MHD models applied to PWNe is the magnetization of the pulsar wind, σ , which determines the fraction of the pulsar spin-down losses that carried by the Poynting flux. This parameter determines the magnetic field at the pulsar wind TS. The downstream magnetic field at the TS is

$$B \approx h(\sigma) \sqrt{\frac{L_{\text{SD}}}{cR_{\text{TS}}^2}} \approx 400h(\sigma) \left(\frac{R_{\text{TS}}}{0.1 \text{ pc}} \right)^{-1} \mu\text{G}, \quad (6)$$

where the function h accounts for the Rankie-Hugoniot conditions at the TS and the strength of the magnetic field in the unshocked pulsar wind: $h \approx 1$ for $1 > \sigma \geq 0.1$, and $h(\sigma) \approx 3\sigma^{1/2}$ for $\sigma < 0.1$. In the case of the Crab Nebula, the radius of the termination shock is constrained robustly, $R_{\text{TS}} \lesssim 0.1 \text{ pc}$, with the observations in the X-ray band (Weiskopf et al. 2000), the magnetic field at the TS should exceed $100 \mu\text{G}$, unless the wind magnetization is very small, $\sigma \leq 10^{-2}$, or magnetic field dissipates at the TS (Lyubarsky 2003; Sironi & Spitkovsky 2011).

As shown in Fig. 3, the strength of the magnetic field in the region responsible for acceleration of the “wind electrons” should not exceed $125 \mu\text{G}$. Eq. (6) shows that such a modest magnetic field requires very weak magnetization of the pulsar wind, $\sigma \leq 10^{-2}$. Although 1D MHD models of the Crab Nebula, does require such a weakly magnetized pulsar wind, currently, it is considered as an artefact of the ideal 1D approximation. Indeed, the rigid flow structure implemented in ideal 1D models results in a rapid increase of

the magnetic field in the shocked pulsar wind. The initially weak magnetic field in the flow approaches the equipartition strength on the scale of several termination shock distances. For the magnetization of $\sigma = 3 \times 10^{-3}$, simple 1D models can reproduce the radiation spectrum (Kennel & Coroniti 1984), expansion rate, and, to some extent, also the X-ray morphology band (Bogovalov & Khangulyan 2002).

3D MHD models agree better with the features of the Crab Nebula if one adopts a higher wind magnetization. As revealed by numerical simulations, the initially strong magnetic field can dissipate significantly in the shocked pulsar wind, allowing MHD solutions with highly magnetized pulsar winds, $\sigma \sim 0.5$. However, such a strong magnetization implies strong magnetic field at the TS, $B \approx 400 \mu\text{G}$. The estimate based on Eq. (6) is consistent with 3D numerical simulations by Porth et al. (2014). If UHE electrons were accelerated in a region with such a strong magnetic field, their synchrotron emission would violate the level of the MeV flux. In Fig. 11 (right panel) of Porth et al. (2014) one can see a small region close in the equator plane characterized by a relatively weak magnetic field. Actually, the equatorial region has been suggested as the most plausible site for the acceleration of TeV electrons in the Crab Nebula (Sironi & Spitkovsky 2011; Olmi et al. 2015), but a highly anisotropic pulsar wind might be required to supply enough energy to this relatively compact region.

4 CONCLUSION

The energy-dependent morphology seen in the center part of the Crab Nebula suggests that the TeV electrons originate at the pulsar wind TS. The IC emission of these very high-energy electrons smoothly extends to the UHE regime as shown by the recent *Tibet ASy* measurements. Since UHE electrons predominately interact with CMBR photons, their spectrum and the total energetics is derived model-independently. Because of the short cooling time, these electrons are confined in the proximity of the accelerator. The joint analysis of the fluxes of synchrotron and IC components reveals a weak magnetic field, $\leq 120 \mu\text{G}$, in the acceleration site responsible for acceleration of multi-hundred TeV electrons in the Crab Nebula. To obtain such a weak magnetic field at the pulsar wind TS, one needs either to assume a small magnetization of the pulsar wind, $\sigma \leq 10^{-2}$ or a highly anisotropic pulsar wind and efficient magnetic field reconnection operating at the TS/bulk of the nebula. Either of these possibilities needs to be tested against realistic 3D MHD simulations of the Crab Nebula.

The obtained limitation on the magnetic field might be not valid in the region responsible for acceleration of PeV electrons in the Crab Nebula. The future observations above 1 MeV and 300 TeV will reveal the physical conditions in that region. In particular, these observations have a potential (1) to verify if the broad band spectrum requires a presence of an additional electron component with a narrow energy distribution, and (2) to constrain the magnetic field strength in the region responsible for acceleration of the PeV electrons.

If this future study favors a strong magnetic field in the region of acceleration of PeV electrons, which are responsible for the $\sim 100 \text{ MeV}$ steady emission in the Crab Nebula, then the site(s) of acceleration of this component could

be responsible also for the enhanced GeV emission observed during the Crab flares. Thus, the future observations of UHE gamma rays up to 1 PeV may shed light on the origin of this component, and, perhaps also, its links to the Crab flares.

ACKNOWLEDGEMENTS

The authors thank V.Bosch-Ramon and anonymous referee for their useful comments. DK is supported by JSPS KAKENHI Grant Numbers JP18H03722, JP24105007, and JP16H02170. M.A. is supported by the RIKEN Junior Research Associate Program.

REFERENCES

Abdalla H., et al., 2019, *Nature Astronomy*, p. 476
 Abdo A. A., et al., 2011, *Science*, 331, 739
 Abeysekara A. U., et al., 2019, *ApJ*, 881, 134
 Aharonian F. A., 1995, Nuclear Physics B Proceedings Supplements, 39A, 193
 Aharonian F. A., Atoyan A. M., 1981, *Ap&SS*, 79, 321
 Aharonian F. A., Atoyan A. M., 1998, in Shibasaki N., ed., Neutron Stars and Pulsars: Thirty Years after the Discovery. p. 439 ([arXiv:astro-ph/9803091](https://arxiv.org/abs/astro-ph/9803091))
 Aharonian F. A., Atoyan A. M., Kifune T., 1997, *MNRAS*, 291, 162
 Aharonian F. A., Belyanin A. A., Derishev E. V., Kocharovsky V. V., Kocharovsky V. V., 2002, *Phys. Rev. D*, 66, 023005
 Aharonian F., et al., 2004, *ApJ*, 614, 897
 Aharonian F., et al., 2006, *A&A*, 457, 899
 Aharonian F. A., Kelner S. R., Prosekin A. Y., 2010, *Phys. Rev. D*, 82, 043002
 Albert J., et al., 2008, *ApJ*, 674, 1037
 Amenomori M., et al., 2019, *Phys. Rev. Lett.*, 123, 051101
 Aramaki T., Adrian P. O. H., Karagiorgi G., Odaka H., 2020, *Astroparticle Physics*, 114, 107
 Atoyan A. M., Aharonian F. A., 1996, *MNRAS*, 278, 525
 Atoyan A. M., Nagapetyan A., 1987, *Astrophysics*, 26, 318
 Bai X., et al., 2019, arXiv e-prints, p. [arXiv:1905.02773](https://arxiv.org/abs/1905.02773)
 Barkov M. V., Lyutikov M., Khangulyan D., 2019, *MNRAS*, 484, 4760
 Bogovalov S. V., Khangoulian D. V., 2002, *MNRAS*, 336, L53
 Bogovalov S. V., Khangoulyan D. V., 2002, *Astronomy Letters*, 28, 373
 Bogovalov S. V., Chechetkin V. M., Koldoba A. V., Ustyugova G. V., 2005, *MNRAS*, 358, 705
 Bucciantini N., 2014, *Astronomische Nachrichten*, 335, 234
 Buehler R., et al., 2012, *ApJ*, 749, 26
 Bühler R., Blandford R., 2014, *Reports on Progress in Physics*, 77, 066901
 Camus N. F., Komissarov S. S., Bucciantini N., Hughes P. A., 2009, *MNRAS*, 400, 1241
 Cerutti B., Werner G. R., Uzdensky D. A., Begelman M. C., 2012, *ApJ*, 754, L33
 Cerutti B., Werner G. R., Uzdensky D. A., Begelman M. C., 2013, *ApJ*, 770, 147
 Foreman-Mackey D., Hogg D. W., Lang D., Goodman J., 2013, *PASP*, 125, 306
 He H., 2019, in Proceedings, 36th International Cosmic Ray Conference (ICRC 2019): Madison, U.S.A., July 24-August 1, 2019. p. 693
 Hester J. J., 2008, *ARA&A*, 46, 127
 Jourdain E., Roques J. P., 2009, *ApJ*, 704, 17
 Kennel C. F., Coroniti F. V., 1984, *ApJ*, 283, 710

Khangulyan D., Aharonian F. A., Kelner S. R., 2014, *ApJ*, 783, 100
 Kirsch M. G., et al., 2005, in Siegmund O. H. W., ed., Society of Photo-Optical Instrumentation Engineers (SPIE) Conference Series Vol. 5898, Proc. SPIE. pp 22–33 ([arXiv:astro-ph/0508235](https://arxiv.org/abs/astro-ph/0508235)), doi:10.1117/12.616893
 Komissarov S. S., 2013, *MNRAS*, 428, 2459
 Komissarov S. S., Lyubarsky Y. E., 2004, *MNRAS*, 349, 779
 Kuiper L., Hermsen W., Cusumano G., Diehl R., Schönfelder V., Strong A., Bennett K., McConnell M. L., 2001, *A&A*, 378, 918
 Lyubarsky Y. E., 2002, *MNRAS*, 329, L34
 Lyubarsky Y. E., 2003, *MNRAS*, 345, 153
 Lyutikov M., 2010, *MNRAS*, 405, 1809
 Lyutikov M., Komissarov S., Sironi L., Porth O., 2018, *Journal of Plasma Physics*, 84, 635840201
 Lyutikov M., Temim T., Komissarov S., Slane P., Sironi L., Comisso L., 2019, *MNRAS*, 489, 2403
 Madsen K. K., et al., 2015, *ApJ*, 801, 66
 Meyer M., Horns D., Zechlin H.-S., 2010, *A&A*, 523, A2
 Olmi B., Del Zanna L., Amato E., Bandiera R., Bucciantini N., 2014, *MNRAS*, 438, 1518
 Olmi B., Del Zanna L., Amato E., Bucciantini N., 2015, *MNRAS*, 449, 3149
 Porth O., Komissarov S. S., Keppens R., 2014, *MNRAS*, 438, 278
 Rees M. J., Gunn J. E., 1974, *MNRAS*, 167, 1
 Sironi L., Spitkovsky A., 2011, *ApJ*, 741, 39
 Sironi L., Spitkovsky A., 2014, *ApJ*, 783, L21
 Sironi L., Keshet U., Lemoine M., 2015, *Space Sci. Rev.*, 191, 519
 Tavani M., et al., 2011, *Science*, 331, 736
 Vernetto S., Lipari P., 2016, *Phys. Rev. D*, 94, 063009
 Volpi D., Del Zanna L., Amato E., Bucciantini N., 2008, *A&A*, 485, 337
 Weisskopf M. C., et al., 2000, *ApJ*, 536, L81
 Yeung P. K. H., Horns D., 2019, *ApJ*, 875, 123
 Zabalza V., 2016, in Proceedings, 34th International Cosmic Ray Conference (ICRC 2015): The Hague, The Netherlands, July 30-August 6, 2015. p. 922 ([arXiv:1509.03319](https://arxiv.org/abs/1509.03319)), doi:10.22323/1.236.0922
 Zanin R., 2017, in European Physical Journal Web of Conferences. p. 03003 ([arXiv:1701.07364](https://arxiv.org/abs/1701.07364)), doi:10.1051/epjconf/201713603003
 de Angelis A., et al., 2018, *Journal of High Energy Astrophysics*, 19, 1
 de Jager O. C., Harding A. K., 1992, *ApJ*, 396, 161
 de Jager O. C., Harding A. K., Michelson P. F., Nel H. I., Nolan P. L., Sreekumar P., Thompson D. J., 1996, *ApJ*, 457, 253

APPENDIX A: MARKOV CHAIN MONTE CARLO MODELLING OF THE HARD X-RAY AND MULTI-TeV EMISSION FROM THE CRAB NEBULA

To study the constraints imposed by the UHE gamma-ray spectrum measured from the Crab Nebula, we fitted the *INTEGRAL* and gamma-ray (above 10 TeV) spectra with a synchrotron – IC model. The energy distribution of emitting particles is assumed to be a power-law with exponential cut-off:

$$\frac{dN}{dE} = A \left(\frac{E}{1 \text{ TeV}} \right)^{-\alpha} \exp \left[- \left(\frac{E}{E_{\text{cut}}} \right)^{\beta} \right], \quad (\text{A1})$$

where E is electron energy. The particle spectrum is determined by four parameters: A is normalization; E_{cut} is cutoff energy; α is the spectral index of a power-law distribution;

Table A1. Results of fitting of the hard X-ray and multi-TeV spectra of the Crab Nebula with `naima`.

parameter	value
magnetic field	$B = 118_{-2}^{+3} \mu\text{G}$
normalization	$A = 1.0_{-0.1}^{+0.2} \times 10^{35} \text{ eV}^{-1}$
power-law index	$\alpha = 2.88 \pm 0.04$
cutoff energy	$E_{\text{cut}} = 330 \pm 20 \text{ TeV}$
cutoff index	$\beta = 1.6 \pm 0.2$

and β is the cutoff index. Leptons produce X-ray emission through synchrotron radiation in a magnetic field, which is assumed to have a random orientation but uniform strength B . The gamma-ray emission is generated through IC scattering on CMBR, FIR (a graybody distribution with temperature $T_{\text{FIR}} = 70 \text{ K}$ and energy density $U_{\text{FIR}} = 0.5 \text{ eV cm}^{-3}$), NIR ($kT_{\text{NIR}} = 5000 \text{ K}$, $U_{\text{NIR}} = 1 \text{ eV cm}^{-3}$), and synchrotron photons (assuming a homogeneously generated target). We note that the CMBR photons provide the dominant contribution, so our specific assumptions about the photon targets have only a minor influence on the result.

The computation of the SED models and subsequent fit to the multiwavelength SEDs are performed using the `naima` Python package (Zabalza 2016). Specifically, synchrotron emission is computed based on the formalism in Aharonian et al. (2010), and IC emission on the formalism in Aharonian & Atoyan (1981) and Khangulyan et al. (2014). `naima` allows one to obtain the best-fit values and posterior probability distributions of the model parameters given the SED points from the χ^2 , calculated assuming that the SED point uncertainties are Gaussian and uncorrelated. The model parameters are scanned using the MCMC method, as implemented in the `emcee` package (Foreman-Mackey et al. 2013). For all model parameters we assume a flat prior probability distribution, within physical constraints on the parameters values (e.g., particle densities are positive). We scan the normalization A and the cutoff energy E_{cut} in logarithmic space, so that the fit parameter is actually $\log_{10}(A/\text{eV}^{-1})$ and $\log_{10}(E_{\text{cut}}/1 \text{ TeV})$, respectively.

The fit results are shown in Fig. A1 and summarized in Table A1. Figure A1 contains the probability density distributions of the model parameters, and Table A1 gives median and upper and lower uncertainties on the parameter values. The fitting shows that the hard X-ray and multi-TeV data constrain the magnetic field strength with very high accuracy. As there could be regions with stronger magnetic field in the nebula, lower energy electrons may provide important contribution to the hard X-ray band without producing any sensible IC emission. Thus, one should rather take the *INTEGRAL* measurements as upper limits for the X-ray emission from the zone, where UHE electrons are accelerated, i.e., $B < 120 \mu\text{G}$ in that region.

This paper has been typeset from a TeX/L^AT_EX file prepared by the author.

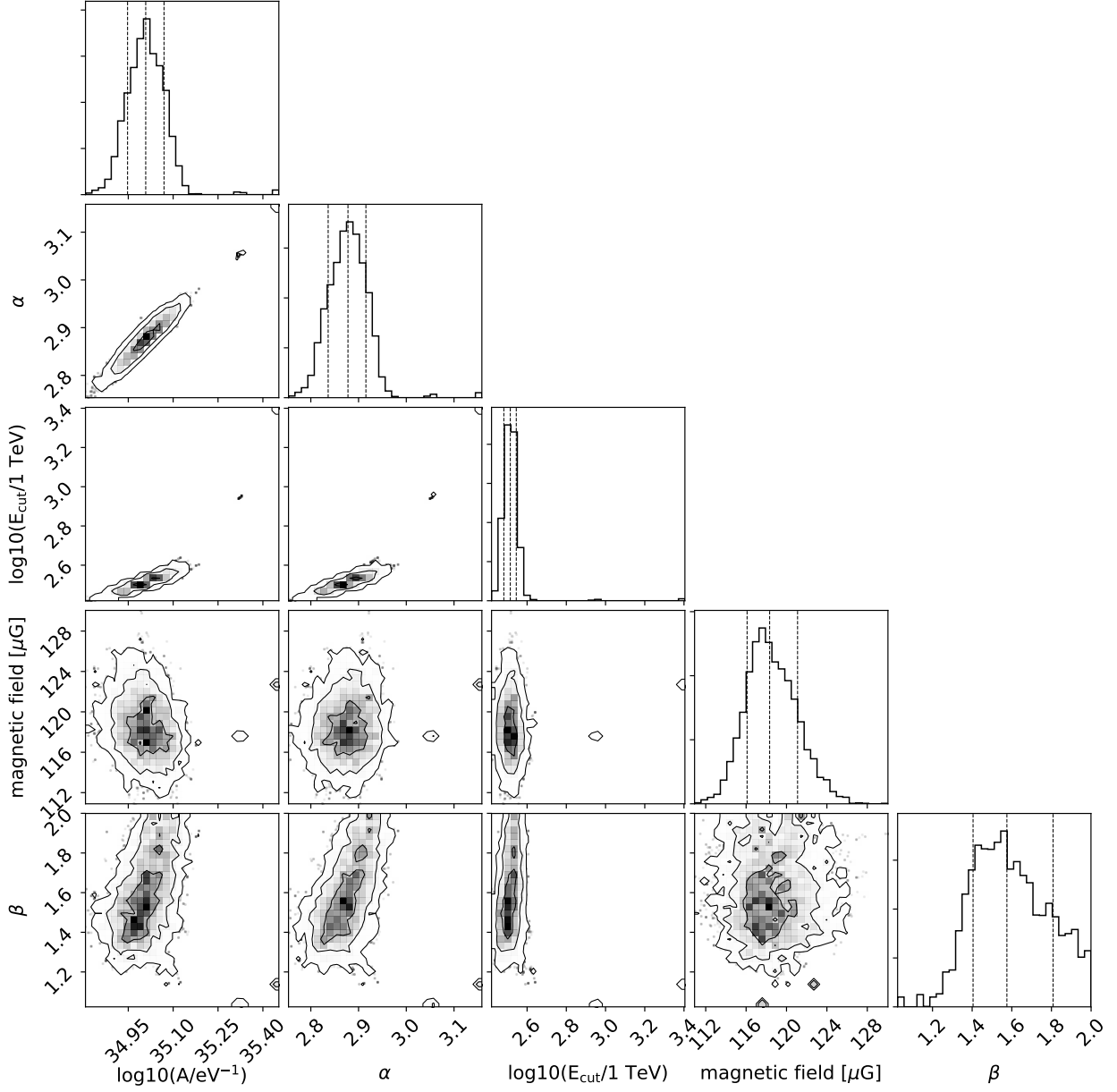


Figure A1. One- and two-dimensional projections of the posterior probability density distributions of the parameters for the radiative model for the hard X-ray and gamma-ray (above 10 TeV) spectra of the Crab Nebula. The parameters of the electron spectrum are defined by Eq. A1. The lines overlaid to the one-dimensional projections are the 16th, 50th and 84th percentiles of the distributions. The contours overlaid to the two-dimensional projections correspond to 1σ , 1.5σ , and 2σ probability decrease with respect to the maximum.